Search for heavy neutrinos in the β-spectrum of ^{63}Ni

E. Holzschuh, W. Kündig, L. Palermo, H. Stüssi, P. Wenk

Physik-Institut der Universität Zürich, CH-8057 Zürich, Switzerland

Abstract

The β-spectrum of ^{63}Ni has been measured with high precision in order to search for effects of heavy neutrinos. For assumed neutrino masses in the range 4 to 30 keV, upper limits of 10^{-3} or less are reported for the mixing probability.

Key words: Neutrino masses; β-spectroscopy.
PACS: 14.60.Pq, 23.40.-s

1 Introduction

The neutrino masses are believed to be very small, of order 1 eV or less. However, direct limits from laboratory experiments, studying the kinematics of suitable decays, are not so small. The present limits for the muon neutrino is 160 keV [1] and for the tau neutrino 18.2 MeV [2].

This is a mass range where β-spectroscopy can contribute solving the problem of neutrino masses, assuming there is also neutrino mixing. In this case, a kink-like structure is expected in an otherwise smooth β-spectrum [3]. This is a unique signature, provided it is measured with high resolution. Besides the known neutrinos, sterile neutrinos may also be searched for.

In this letter, we present high precision measurements of the ^{63}Ni β-spectrum. This is a first set of data, which we have taken to search systematically for neutrino masses and mixing in β-decay.

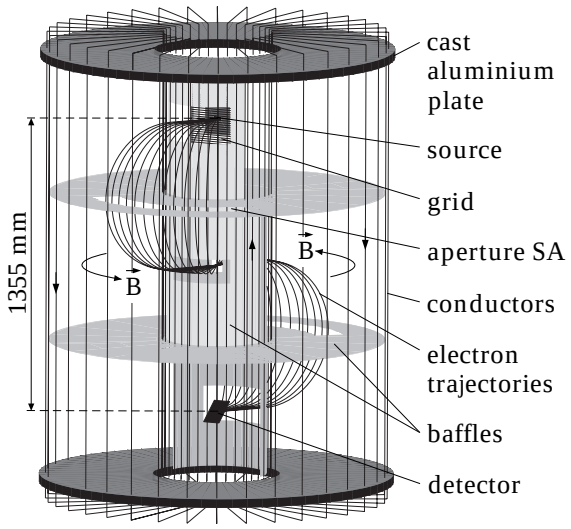

Fig. 1. Simplified view of the spectrometer.

2 Spectrometer

The instrument used in this investigation is an iron-free magnetic β-spectrometer of the Tret'yakov type with electrostatic acceleration. It is a completely redesigned version of a spectrometer previously used to measure the endpoint region of the tritium β-spectrum [4]. A simplified overview is shown in Fig. 1. A toroidal magnetic field is produced by a set of 72 rectangular current loops. Electrons from the source are transported in two 180° bends to the detector. A more detailed description may be found in Ref. [5].

The ^{63}Ni source was mounted on a flat source holder (see below) and placed on the spectrometer axis. The source holder was surrounded by a box-like grid of aluminium wire (98.25 % optical transmission). An electrostatic acceleration field between source holder and grid was produced by applying a negative high voltage V_S to the source holder while keeping the grid at a potential near ground.

The spectrometer has a focal plane which forms an angle of 48.5° with respect to the spectrometer axis. Electrons arriving at the focal plane were detected using a large silicon strip detector consisting of four silicon plates with a sensitive area of $8.0 \times 3.05\,\mathrm{cm}^2$ each. The strip pitch and thus the position resolution was 1.27 mm.

Each detector strip was read out by a separate electronic channel, consisting of a charge sensitive preamplifier, a shaping amplifier (time constant $1\,\mu$s) and an 11 bit ADC. The dead time was measured to be $9.4 \pm 0.3\,\mu$s, being within uncertainties the same for all channels. Electrons, which hit the detector near the borderline of two adjacent strips, thus producing signals in two channels,

were identified with coincidence logic. Some of the detector strips or preamplifiers had excessive noise and were shut off. For each event, pulse height, strip number, and coincidence bits were recorded on magnetic tape.

Measurements were performed by setting the current through the spectrometer coil to a constant analysing energy E_{mag} and by varying the source voltage V_{S} in equal steps. The step size was chosen such that monoenergetic electrons would move by the width of one strip on the detector for each step. The energy range of a measurement was scanned in interlaced up-down sweeps. That means, first V_{S} was set to the low end of the range and an up-sweep was started. After approximately one minute the up-sweep was interrupted and a down-sweep was started at the high end. This was repeated until both sweeps were completed and then started again.

The spectrometer current (and thus E_{mag}) and the voltage V_{S} were measured for each step by integrating over the counting period using precision voltmeters. The earth magnetic field was measured with a three-axes magnetometer and compensated by three sets of large coils to less than 1 mG over the volume of the spectrometer.

Histograms were built off-line from the recorded event data. First, a suitable cut to the pulse height was applied. Events with coincidence bits set were rejected, thus avoiding double counting. Then a position coordinate z along the spectrometer axis with respect to the centre of the detector was determined from the strip number and an energy

$$E = E_{\mathrm{mag}} - e|V_{\mathrm{S}}| + zD_E \tag{1}$$

was assigned to each event. Here, D_E denotes the energy dispersion [5]. The events were summed into bins assuming nominal values for E. The small scatter in the measured values of E_{mag} and V_{S} was taken into account by forming an average of E from all events in a bin. The standard deviation of E was 2 eV or less for all bins, and the error of the average of E could thus be neglected considering the large number of up-down sweeps summed for one histogram.

As E_{mag} was constant during a measurement, electrons which hit the detector at a certain strip, had always the same average energy, independent of V_{S}. Furthermore, each strip measured an independent spectrum and the result of the complete detector was effectively a sum of the partial spectra of all strips. Excepting a small fraction of scattered events [5], the shape of a measured spectrum is thus independent of the detector efficiency.

3 ^{63}Ni source

The source was produced by vacuum evaporation of active, metallic nickel onto a thin foil of polyimide (Kapton). The layout of the source is shown in Fig. 2. In order not to compromise the spectrometer resolution, the source was segmented [6] into 20 strips ($30 \times 0.7\,\mathrm{mm}^2$ each) with 1 mm pitch. The strips were connected to electrical potentials varying linearly in vertical direction (spectrometer axis).

The polyimide foil was produced [7] using the recipe of Ref.s [8,9]. The foil thickness was determined by measuring the energy loss of α-particles (^{241}Am) passing through the foil. A non-uniformity could not be detected. The energy loss per mass layer was computed using the program TRIM [10]. The mass thickness was found to be $(23 \pm 2)\,\mu\mathrm{g/cm}^2$, corresponding to 1600 Å assuming the density of Kapton ($1.42\,\mathrm{g/cm}^3$).

The foil was glued onto a printed board having an opening of $45 \times 21\,\mathrm{mm}^2$ (see Fig. 2). The pattern of electrically conducting strips was produced by evaporating a 200 Å thick layer of aluminium through a mask onto the foil.

The ^{63}Ni activity was purchased as nickel chloride dissolved in hydrochloric acid. The specific activity was 12.8 mCi per 1 mg of nickel. The total amount was 10 mCi. The solution was first dried up to remove the hydrochloric acid. Then the nickel chloride was dissolved in 3.5 molar ammonia solution and filled into a tungsten boat. The chloride was electro-chemically reduced to metallic nickel forming a thin layer in the boat. After rinsing with pure water, the boat was heated to about 600°C in order to remove any volatile contaminants. Then the metallic nickel was evaporated onto the polyimide foil through the same mask as above and an additional aperture.

The activity of the completed source was measured with an ion chamber and found to be 0.43 mCi. This corresponds to a thickness of $8.0\,\mu\mathrm{g/cm}^2$ or 90 Å with an estimated uncertainty of 10 %.

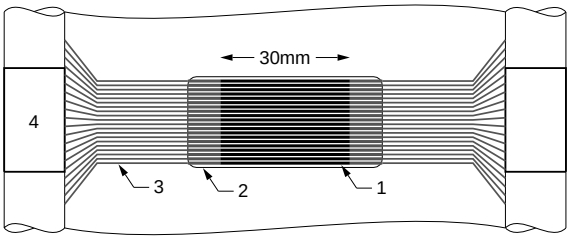

Fig. 2. Layout of the ^{63}Ni source. (1) Active area, (2) thin foil stretched over an opening, (3) electrical connections, (4) insulator and support frame. The vertical direction through the centre coincides with the spectrometer axis.

Radioactive contaminants were examined by measuring characteristic γ-rays with a germanium detector. Traces of ^{60}Co and ^{109}Cd were found and are discussed below.

4 Measurements

4.1 The ^{63}Ni spectrum

Three measurements of the ^{63}Ni β-spectrum were performed, extending over an energy range of 33.0 to 67.8 keV. This range was divided into two parts in order to avoid too large values of the source high voltage. A summary of the settings is given in Tab. 1.

The pulse height resolution for run I was 8.0 keV (FWHM) for a typical strip with the detector cooled to -15°C. This poor performance was mainly caused by large leakage currents of the detector diodes. After run I the silicon plates were replaced and the pulse height resolution improved to 5.5 keV (at 0°C). All subsequent measurements were performed with the new plates. Except for the different detector plates the settings of runs I and II were the same.

The energy range of a run was subdivided into several regions in order to compensate somewhat the strongly varying count rate. For runs I/II the counting time per step was 5 s for energies below 55 keV, 7 s for energies in the range 55 to 65 keV, and 9 s above 65 keV. For run III 6 s was used below 44 keV and 12 s above.

The different counting times were taken into account during histogram build-

Table 1
Settings of the measurements of the ^{63}Ni β-spectrum. The pulse height cuts are lower limits used in the analysis and are referred to in the text as cuts 1,2,3 for runs I/II and similarly for run III.

Run no.	I/II	III
Energy range (keV)	44.0 – 67.8	33.0 – 52.0
E_{mag} (keV)	71.5	54.5
Resolution, FWHM (eV)	91.0	70.3
Dispersion (eV/mm)	61.5	47.5
Bin width (eV)	52.0	40.0
Pulse height cuts (keV)	34, 45, 56	23, 40, 46

Table 2
Summary of counts and rates for the measurements of the ^{63}Ni β-spectrum (cut 2).

Run no.	I	II	III
Total counts (10^9)	2.5	1.4	1.3
No. up-down sweeps	694	395	97
Max. rate / strip (s^{-1})	52	52	75
Background / strip (s^{-1})	0.007	0.007	0.024

ing. The number of counts was scaled with the counting times such that the scale factor was 1 at high energies. Histograms were built using three different cuts to the pulse height. The lower limits are given in Tab. 1. The upper limits were chosen to include all signal counts given the pulse height resolution of the detector. Besides reducing the background rate, larger cut values imply the suppression of events where electrons were backscattered from the detector depositing only part of their energy.

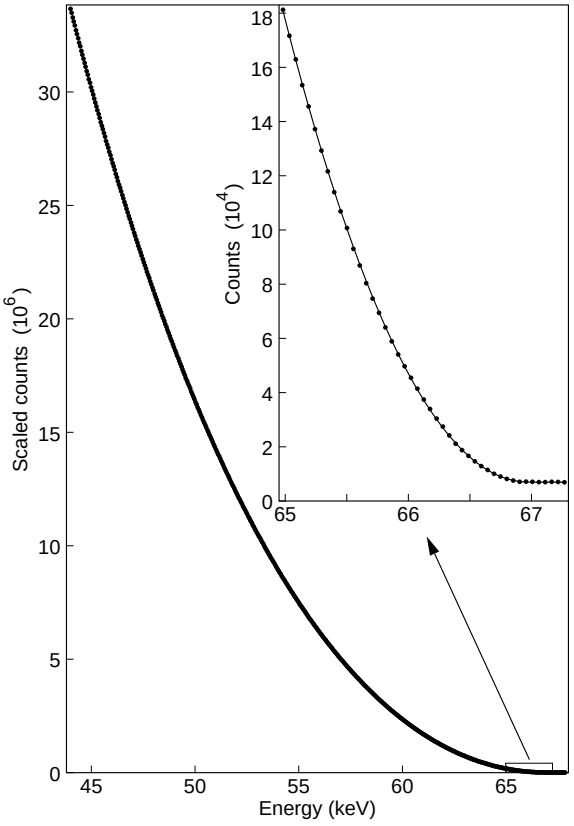

Fig. 3. Measured spectrum of run I (cut 2) and best fit. The inset shows the endpoint region with the vertical scale expanded by approximately a factor 100. All error bars, also in the inset, are much smaller than the size of the data points.

The total number of events is 5.4×10^9 for the three runs. More details are given in Tab. 2. The rates given apply for cut 2 and were obtained by averaging over the complete detector and normalizing to one detector strip. Cut 2 was defined to be the standard cut in the analysis. The data of run I are plotted in Fig. 3. Plotted are scaled counts as explained above. The inset shows the data near the endpoint (67 keV) where the scale factor was 1.

4.2 Backgrounds

The rates of most conceivable sources of background are expected to be energy independent as only the source potential was varied while scanning a spectrum. One exception could be an active contamination of the source holder or foil, e.g. by ^{14}C. To test this possibility, a separate background measurement with a dummy source was performed. Source holder and foil were made in the same way as for the ^{63}Ni source except that non-active nickel was used. The settings were basically the same as for runs I/II but the energy range was extended down to 33 keV.

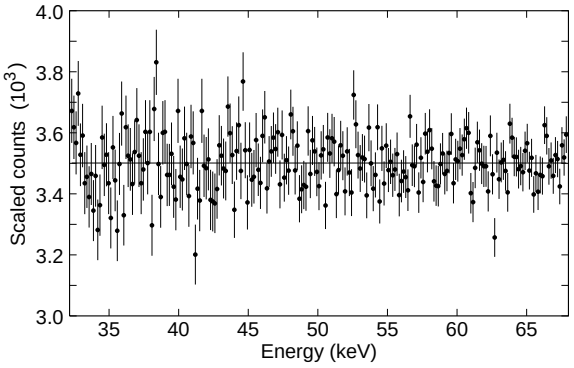

Fig. 4. Measured background with a dummy source. Three bins were added for this plot. The error bars at lower energies are larger because of smaller measuring times.

The result of 115 up-down sweeps (about 14 days of measuring time) is shown in Fig. 4. There is no indication of a variation with energy and the data are well fitted by a constant ($\chi^2 = 687.4$ for 686 degrees of freedom).

The rate measured with the background run and the background as determined from the ^{63}Ni runs I/II at energies above the endpoint agreed within an uncertainty of 2 %. As the endpoint energy of ^{60}Co (318 keV) is larger than of ^{63}Ni, an upper limit for the ^{60}Co contamination of the ^{63}Ni source could be estimated. For the ratio of β-activities we find $A(^{60}\mathrm{Co})/A(^{63}\mathrm{Ni}) < 4 \times 10^{-7}$. Noting that the β-spectrum of ^{60}Co varies by less then 10 % over the measured range, this is negligible.

In the data of runs I and II, a small peak was detected at $E = 62.25$ keV, which coincides with the energy of the K conversion line of ^{109}Cd. The peak height

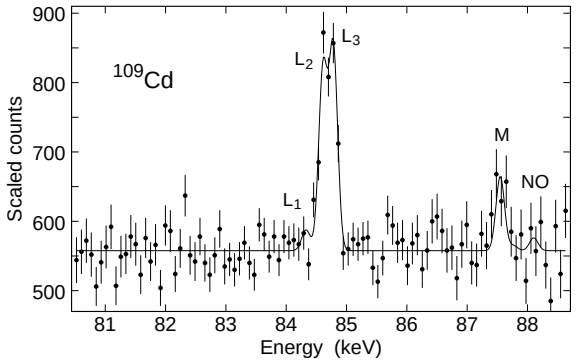

Fig. 5. Measured conversion line spectrum of ^{109}Cd contamination (points) and best fit (line).

was approximately eight standard deviations. To verify this identification, a measurement over an energy range containing the L and M lines of ^{109}Cd was performed. The data are plotted in Fig. 5 and clearly show the L_2 and L_3 lines. The M lines are also significant but not resolved. The data were fitted assuming the line shapes to be given by the computed spectrometer resolution function for this setting ($E_{\mathrm{mag}} = 117.2\,\mathrm{keV}$). The relative line intensities and the energy differences of the lines were taken from the literature [11,12]. A good fit was obtained. Besides unambiguously confirming the ^{109}Cd contamination, this measurement showed the reliability of the computed spectrometer resolution and served as a check of the energy calibration of the spectrometer. Indications for any other active contamination of the ^{63}Ni source were not found.

5 Analysis and results

The very high statistical precision of the data required to take many effects into account. We first discuss the theoretically expected ideal shape of the ^{63}Ni β-spectrum and then corrections specific to the experiment.

5.1 Theoretical spectrum shape

The data were analysed assuming a two-state neutrino mixing scheme with neutrino masses m_1 and m_2. For this case, the β-spectrum is expected to have the form [3]

$$f_m(E) = (1 - |U_{e2}|^2) f(E_0, m_1, E) + |U_{e2}|^2 f(E_0, m_2, E) \qquad (2)$$

It was further assumed that one mass is small, which was taken to be m_1, and that the other mass m_2 is much larger. The mixing probability $|U_{e2}|^2$ must

then be a small number and β-decay must be dominated by the branch with mass m_1. Considering the tight limits from recent tritium experiments [13], m_1 could safely be set zero.

The function $f(E_0, m, E)$ describes a β-spectrum without mixing for a neutrino mass m, an extrapolated endpoint E_0, and kinetic energy E. It was computed in the following way.

The Fermi function for a point charge nucleus with infinite mass is known exactly [14]. The corrections for finite nuclear size and recoil were computed using the accurate parameterization in Ref. [15]. The relative variation of the combined corrections over the measured energy range is 2.2×10^{-4}.

Radiative corrections are known only for zero neutrino mass. To order α, there is a mild logarithmic singularity at the endpoint [16]. Besides this, the correction varies by approximately 3×10^{-3} over the range where the measured spectrum is significantly above background.

Electrostatic screening due to the atomic electrons was taken into account using the Rose prescription [17] with a screening potential of 3.5 keV. The correction agrees with tabulated values [18] within the precision of the table (10^{-4}). The variation is 6×10^{-4}.

The exchange correction arises because β-particles and atomic electrons are indistinguishable [19]. Experimentally, this effect was observed just recently [20], also in the β-spectrum of ^{63}Ni. The exchange correction is surprisingly large, varying by 7×10^{-3} between 33 keV and the endpoint.

The excitation of atomic electrons is a well known effect in tritium β-decay. For other cases it has usually been neglected in the past. Because of our combination of high statistical precision and high instrumental resolution, it was not at all negligible. The distribution of excitation energies was computed for an isolated atom [21] using the same method as in Ref. [22]. The mean excitation energy of the computed distribution was 65 eV, approximately 20 eV lower than what would be expected from a relatively easy to evaluate sum rule (85 eV). We have made a corresponding correction to the distribution, but as this is not unique, it constitutes a major systematic uncertainty.

5.2 Experimental corrections

The acceleration at the source implies that the solid angle accepted by the spectrometer before acceleration increases with increasing source voltage. This effect was studied by Monte Carlo simulation and is well described by the

correction factor [5]

$$S(E) = \frac{Z}{\varphi} \arcsin(Z \sin \varphi), \tag{3}$$

provided the source voltage is limited such that approximately $S \leq 1.7$. Here $Z := p_{\mathrm{mag}}/p$ is the ratio of the spectrometer momentum setting and the momentum at the source, and φ is an effective opening angle. As it was not possible to achieve with the simulation the same precision as experimentally, φ was treated as a free parameter in the analysis.

The spectrometer resolution function was determined by Monte Carlo simulation (for the width see Tab. 1) and taken into account by convolution with the expected spectrum shape.

The energy loss in the source layer was described by a distribution depending on the intial energy of a β-particle and the energy with which the particle left the source. The distribution was determined in the following way. The differential cross sections for K and L excitations in nickel were computed using the programs from Ref. [23]. For the cross sections of the more weakly bound electrons, the model of Ref. [24] was used. At a typical initial energy of 50 keV, the probability that an electron left the source without interaction was found to be 85 % and the mean energy loss was 19 eV. Multiple scattering in the source could thus be neglected. The mean energy loss per path length agreed with tabulated values [25] to within few percent.

Scattering in the spectrometer was investigated experimentally by accelerating photo electrons and by Monte Carlo simulation. Agreement was found within 15 % or better [5]. For the present experiment, the measurements were closely simulated but assuming a source with a spectrum constant in energy. The simulated scattered events were scaled with the expected shape of the ^{63}Ni β-spectrum and then normalized with all events. The probability distribution was suitably parameterized to smooth the statistical fluctuations of the simulation, scaled with the total number of measured events and then added to the fitted function as a fixed correction. The integrated probability for a detected electron being scattered somewhere in the spectrometer was 1.66×10^{-3} for runs I/II and 1.44×10^{-3} for run III.

Lost events due to electronic dead time was taken into account by the appropriate correction factor. As the rate per detector strip was small (see Tab. 2) this correction was at most 7×10^{-4}.

The K conversion line of ^{109}Cd affected significantly two data points in runs I/II and was represented by the resolution function convoluted with the energy loss distribution.

Table 3
Results of the standard fit for cut 2, assuming no mixing and comparison of the effective opening angle φ with the result of Monte Carlo (MC) simulations. The errors are statistical standard deviations.

Run no.	I	II	III
χ^2	522.9	443.8	451.8
NoDF	454	454	473
$E_0 - 66000\,\mathrm{eV}$	980.4 ± 0.4	971.5 ± 0.6	997.4 ± 4.6
φ (Fit) (deg)	19.2 ± 0.1	19.8 ± 0.2	24.1 ± 0.3
φ (MC) (deg)	18.5 ± 1.2	18.5 ± 1.2	23.2 ± 0.4

5.3 Results and discussion

The ^{63}Ni data were first fitted assuming no mixing and using the model function as defined above. Free parameters were a spectrum amplitude, a constant background, endpoint energy E_0, effective opening angle φ, and amplitude and energy of the ^{109}Cd K line. Phenomenological 'shape correction factors', as often used in β-spectroscopy, were not necessary. The three data sets were fitted independently and the results for pulse height cut 2 are given in Tab. 3. The results for other cuts were quite similar.

The fitted values of E_0 show a scatter, much larger than the statistical errors. These systematic variations are caused by uncertainties of the axial positions of source and detector, the reproducibility of both being about 0.1 mm. This translates in a calibration error of approximately 10 eV. Including the calibration uncertainty of the spectrometer current and taking an average, we find

$$E_0 = 66980 \pm 15\,\mathrm{eV}. \tag{4}$$

This result is compatible with a measurement which we have performed previously [26] but is larger than the values obtained recently by others: 66946 ± 20 eV [27] and 66945 ± 4 eV [28]. The discrepancy is explained by the fact that in those works the excitation of atomic electrons was not taken into account. This neglect forces a fit to an endpoint which is too small by an amount of the order of the mean excitation energy (85 eV).

The values of the opening angle φ from the fit and from Monte Carlo simulations are compared in Tab. 3. Within uncertainties there is agreement between the two sets of values.

If the exchange correction factor is omitted, the fitted value of φ increases

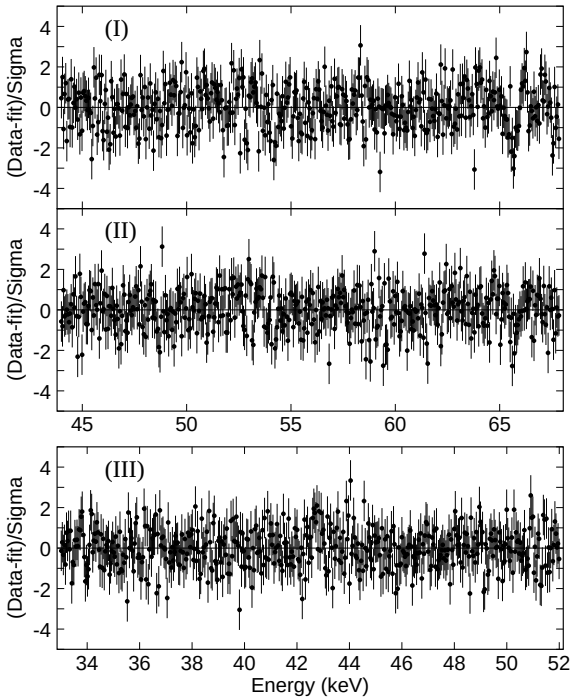

Fig. 6. Data minus the best fit divided by the statistical standard deviation for the three ^{63}Ni runs (cut 2 and no mixing).

by 2.2° for all three data sets, thus causing a discrepancy with the simulated values. In this sense we can confirm the observation of the exchange effect in Ref. [20].

The differences between the data (cut 2) and the fitted model (no mixing), normalized with the standard deviations are plotted in Fig. 6. Over most of the energy range there is very good agreement. This is also indicated by the values of χ^2 in Tab. 3, being statistically acceptable. However, in an approximately 2 keV wide interval below the endpoint, significant deviations can be recognized for run I and to a smaller extent also for run II.

This discrepancy is likely to be caused by the computed excitation probabilities being not as accurate as required by the data. The typical energy of the deviations suggests that the excitations of L electrons (threshold 931 eV) are of particular importance. The integrated probability for these was computed to be 2 %. To set this into perspective, the relative error of each data point near 1 keV below E_0 is about 4×10^{-3}. The computed probabilities for more weakly bound electrons are believed to be more accurate. Moreover, such excitations affect the spectrum shape only close the endpoint where the precision of the data is smaller. The probabilities for excitations involving K electrons were computed to be small (total 0.2 %), but not quite negligible.

Neutrino mixing was searched for by a combined fit of the three data sets with one common free parameter for the mixing probability $|U_{e2}|^2$ (see Eq. (2)). The

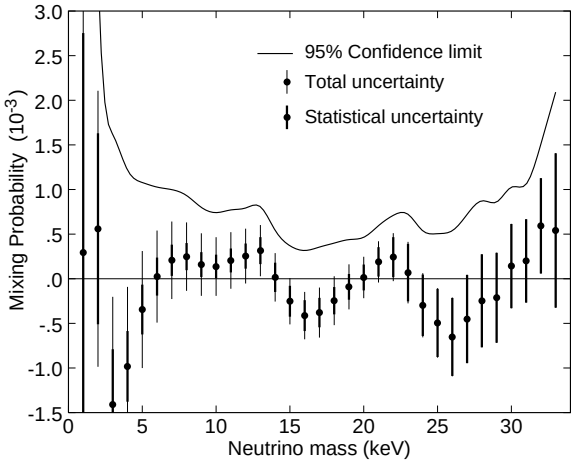

Fig. 7. Best fit (points) of the mixing probability as a function of assumed neutrino mass. The error bars combine statistical and systematic errors. The thick part of the error bars represents the statistical errors only. The solid line is an upper limit at 95 % confidence.

assumed neutrino mass m_2 was varied in steps up to 33 keV. The results are shown in Fig. 7. There is no indication for neutrino mixing in this range. We note that the points in Fig. 7 are not statistically independent as they are derived from the same data. As a consequence, the fitted value of $|U_{e2}|^2$ varies in a highly correlated way as a function of m_2.

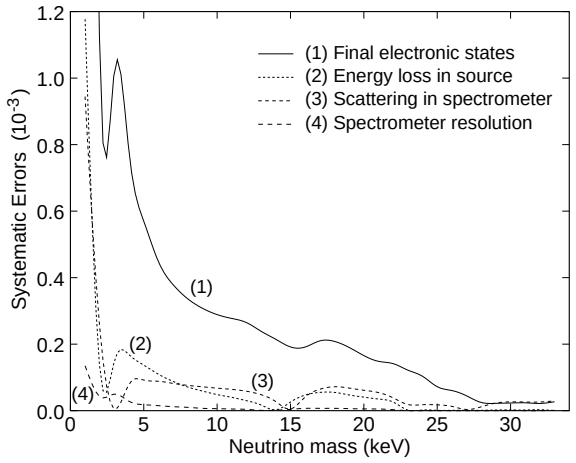

Fig. 8. Estimate of systematic errors (1σ) of the mixing probability as a function of the assumed neutrino mass.

Systematic uncertainties for $|U_{e2}|^2$ were determined by varying the various corrections in the fitted model and fitting the data again. The differences to the standard model were taken as 1σ errors. The results are plotted in Fig. 8.

The experimental systematic uncertainties, although estimated conservatively, were found to be small, for $m_2 \geq 2\,\mathrm{keV}$ less than 2×10^{-4}. Uncertainties due to the spectrometer resolution function were determined by varying its width by 5 %. This could have been neglected. Energy loss in the source was varied

by changing the source thickness within 20 %. The amplitude of the correction for scattering in the spectrometer was varied by 25 %. This correction depends on the pulse height cut and could thus be tested by fitting the data also with cuts 1 and 3. With respect to the standard cut 2, the differences of $|U_{e2}|^2$ were always smaller than one half of the statistical standard deviations. This is consistent with statistical fluctuations as the cuts changed the number of events in the data by some 15 %.

From possible theoretical uncertainties only those due to the excitation probabilities were considered as these seem to be dominant. The probabilities and energies for L and K excitations were changed in various ways but such that the mean excitation energy remained constant, consistent with the sum rule. The differences to the standard model were taken as 1σ errors. In addition, fits with the uncorrected distribution were performed and compared with the standard model. For this case, one half of the differences was taken as a further error as this correction is theoretically well justified. Then, all errors were combined quadratically. The result is shown in Fig. 8 as curve (1).

The statistical and all systematic uncertainties were added quadratically. The total uncertainties are plotted in Fig. 7 as thin error bars. Upper limits for the mixing probabilities at 95 % confidence were computed using the method of the particle data group [29]. The result is shown in Fig. 7. At $m_2 = 1\,\mathrm{keV}$, the limit is 1.2×10^{-2} and then drops quickly to a level around 10^{-3} or below.

6 Conclusion

We have presented high precision measurements of the ^{63}Ni β-spectrum. Indications for neutrino mixing were not found. For assumed neutrino masses in the range 4 to 30 keV, limits for the mixing probability at 10^{-3} or less were determined. For smaller neutrino masses the limits could be improved with more accurate excitation probabilities.

The experiment was also a precise test of β-decay theory, which turned out to be amazingly accurate considering all the theoretical corrections which had to be taken into account. The recently observed exchange effect was confirmed.

Acknowledgements

This work has been supported by the Swiss Science Foundation and by the Paul Scherrer Institute (PSI) which is gratefully acknowledged. We thank S.

Schafroth for performing the calculations of the excitation probabilities and R. Alberto for help making the source.

References

[1] K. Assamagan et al., Phys. Rev. D 53 (1996) 6065.

[2] R. Barate et al. (Aleph Collab.), Euro. Phys. J. C 2 (1998) 395.

[3] R.E. Shrock, Phys. Lett. 96B (1980) 159.

[4] E. Holzschuh, M. Fritschi, W. Kündig, Phys. Lett. B 287 (1992) 381.

[5] E. Holzschuh, W. Kündig, L. Palermo, H. Stüssi, P. Wenk, Nucl. Instr. Meth. A, in print.

[6] K.E. Bergkvist, Nucl. Phys. B 39 (1972) 317.

[7] P. Wenk, Dissertation, University of Zürich, 1998.

[8] J. Pauwels et al., Nucl. Instr. Meth. 167 (1979) 109.

[9] P. Maier-Komor, Nucl. Instr. Meth. A 282 (1989) 172.

[10] J.P. Biersack, J.F. Ziegler, Computer program TRIM, IBM, 1989.

[11] C.M. Lederer et al., Table of isotopes, 7th Ed., John Wiley & Sons, NewYork, 1978.

[12] O. Dragoun et al., Z. Phys. A 279 (1976) 107.

[13] C. Caso et al. (Particle Data Group), Euro. Phys. J. C 3 (1998) 1.

[14] H. Behrens, W. Bühring, Electron Radial Wave Function and Nuclear Beta-decay, Clarendon Press, Oxford, 1982.

[15] D.H. Wilkinson, Nucl. Instr. Meth. A 290 (1990) 509.

[16] A. Sirlin, Phys. Rev. 164 (1967) 1767.

[17] M. Rose, Phys. Rev. 49 (1936) 727.

[18] H. Behrens, J. Jaenecke, in Landolt-Börnstein, New Series, Vol. 4, Numerical tables for beta-decay and electron capture, Springer Verlag, Berlin, 1969.

[19] M.R. Harston, N.C. Pyper, Phys. Rev. A 45 (1992) 6282.

[20] L.C. Angrave et al., Phys. Rev. Lett. 80 (1998) 1610.

[21] S. Schafroth, University of Zürich, private communication.

[22] T.A. Claxton, S. Schafroth, P.F. Meier, Phys. Rev. A 45 (1992) 6209.

[23] R.F. Egerton, Electron energy loss spectroscopy in the electron microscope, 2nd Ed., Plenum Press, New York, 1996.

[24] D. Liljequist, J. Phys. D 16 (1983) 1587.

[25] M.J. Berger, S.M. Selzer, ICRU report 37, 1984.

[26] E. Holzschuh, W. Kündig, Proc. 13th Moriond Workshop (Villar sur Ollon, 1993), ed. J. Tran Than Van et al., Editions Frontières, France, p. 329.

[27] D.W. Hetherington et al., Phys. Rev. C 36 (1987) 1504.

[28] H. Kawakami et al., Phys. Lett. B 287 (1992) 45.

[29] H. Hikara et al. (Particle Data Group), Phys. Rev. D 45 (1992) III.32.